Atomistic theory of the interaction between AFM tips and ionic surfaces

1994 J. Phys.: Condens. Matter 6 1825

(http://iopscience.iop.org/0953-8984/6/10/003)

J. Phys.: Condens. Matter 6 (1994) 1825–1846. Printed in the UK

Atomistic theory of the interaction between AFM tips and ionic surfaces

A L Shluger†‡, A L Rohl†, D H Gay† and R T Williams§

† The Royal Institution of Great Britain, 21 Albemarle Street, London W1X 4BS, UK
‡ Department of Chemical Physics of Condensed Matter, University of Latvia, 19 Rainis blvd, Riga, 1098 Latvia
§Department of Physics, Wake Forest University, Winston-Salem, NC 27109, USA

Received 27 September 1993, in final form 24 January 1994

Abstract. The interactions between an atomic force microscope (AFM) tip and the perfect and defective (001) surfaces of LiF, NaCl and CaO have been studied by quantum-chemical and atomistic simulation techniques. The liquid which is usually present on surfaces in experimental conditions, is considered to be inert and not contributing to the imaging. However, its chemical interaction with the tip is taken into account via the specific microscopic structure of the very end of the tip, reflecting the possibility of its oxidation and protonation. Calculations were performed for three models representing the nano-asperity at the end of SiO_2 and MgO tips consisting of up to 66 atoms. The tip–surface interaction and related forces were calculated as a function of the chemical structure of the tip, its shape, and its distance from the surface. The associated tip and surface distortions caused by this interaction were investigated. We studied the atomic structure of Mg and O impurity defects near the (001) LiF surface, and OH^- molecular ion substituting for Cl on the (001) surface of NaCl, and calculated their stability, adiabatic barriers for diffusion, and AFM images. It is demonstrated that the optimal tip–surface distance for 'atomic resolution' is about 3–5 Å, which corresponds to the presence of one or two liquid layers between the tip and the surface. The surface and defect distortion by the tip is small in this distance range and greatly increases at smaller distances, leading to creation of surface defects. The electrostatic contribution to the tip–surface interaction makes a basis for 'atomic resolution' at large distances, whereas much stronger 'chemical' interactions dominate at small distances. The results suggest that it should be possible to image charged impurities such as Mg or O ions substituting for the host ions in alkali halides by AFM.

1. Introduction

The atomic force microscope (AFM) [1,2] is a tool originally intended for investigating the atomic structure of non-conducting surfaces and the microscopic forces between the atoms of the tip and the surface. These forces are similar to those which determine adhesion, friction and other properties of interfaces. It was expected to parallel the success of the STM as a powerful means for studying surfaces with 'atomic resolution'. Despite the growing number of publications demonstrating the structures of various periodic and non-periodic systems (see [3–5] for recent reviews), some basic problems regarding the possibility of obtaining true atomic resolution still remain unresolved. In particular, since the distance between the tip and the surface of the AFM is not controlled by the feedback loop, the van der Waals interaction between the macroscopic tip and the surface tends to pull them together with a force which is hardly sustainable by both systems if they are in contact in vacuum or in air [6]. This leads to a strong surface distortion, with the tip essentially dragging along

0953-8984/94/101825+22$19.50

the surface during scanning [5–8]. There are, therefore, no conclusive AFM experiments demonstrating atomic resolution in UHV or in dry air so far.

Recent experimental studies have demonstrated, however, that by controlling the humidity in the experimental chamber or by doing experiments in liquid [9], one can obtain true atomic images of periodic surfaces and step edges [8,10]. Several images of 'point defects' have also been reported [8,11]. The presence of liquid apparently makes the tip–surface interaction less destructive. In particular, the layer of adsorbed molecules or embedding media reduce the van der Waals interaction [12,13]. Besides, in the case of relatively small applied forces, the tip does not poke through the liquid layer, and the tip-surface separation effectively increases. In combination with using ultra-sharp tips [14], reducing the van der Waals force, and very sensitive cantilevers, it appears to be possible to measure tip-surface forces as small as several pN [10,15]. It is assumed that the liquid itself is not imaged, although it may oxidize or protonate the tip, produce a charged double-layer and dissolve the surface and considerably change the surface transport properties. Good atomic images have been obtained in humid air for the soft hydrophilic surfaces of ionic alkali halides [5,7,8], and under liquid for SrF_2 [16] and calcite [10]. The first group of experiments has been performed in a repulsive constant force mode of observation, where the force exerted on the cantilever was about 10–200 nN. In the latter case the variable-deflection mode was used, where the lever deflection was caused by a very small attractive force of about 20 pN with no hysteresis observed in the force versus distance curves. Note that the forces measured on the cantilever are not equivalent to those acting between the nano-asperity at the end of the tip and the surface. They represent the balance between the cantilever bending force and the other forces between the macroscopic tip and the sample, and depend on the experimental set-up. Recent calculations [8] suggest that if the resulting force at the very end of the tip is larger than several nN, the tip–surface interaction is most likely damaging the surface.

These results clearly demonstrate that large van der Waals and capillary forces (encountered when imaging in humid air) [12], which attract the tip to the surface, can be effectively reduced by bulk liquid or distributed by surface coverage of many molecules. In the latter case these forces are apparently counterbalanced by the presence of a soft lubricant layer between the tip and the surface. It is interesting to note that the resulting cantilever forces measured in [10,15] have the same order of magnitude as those predicted theoretically for the 'chemical' interaction of the nano-asperity at the end of the tip with the ionic surfaces [8,17,18]. It seems, therefore, plausible to assume that observed images are primarily determined by electrostatic and short-range 'chemical' forces acting between the atoms at the very end of the tip and the surface atoms.

Some related issues have been considered in several recent model studies [19]. However, calculations treating realistic tips and surfaces are still rare. Although these are more specific than model studies, if they are performed on different tip models and surfaces, they can reveal important general trends. Furthermore, recent development of simulation techniques and their successful application to studies of very complicated systems [20] suggests that the successful interpretation of experimentally obtained images will depend on the direct simulation of real AFM operation in the near future. Extensive simulation work has been already performed by Landman and coworkers on metal tips interacting with metallic surfaces [21] using molecular dynamics techniques. These calculations and the work of Sutton *et al* [22] highlighted the importance of adhesion, the effects of friction and wear, and the hysteresis of the force versus distance behaviour in the case of surface indentation. Our main interest is in ionic crystal surfaces, such as alkali halides and oxides, where electrostatic forces play a decisive role. Girard *et al* [17] and Giessibl [18] have

considered some of these forces. In particular, [18] used an oxygen atom as a model tip interacting with the (001) KBr surface. It was demonstrated that a polarizable atom simulating the very end of the tip, placed in the non-uniform surface electric field at a distance of 3–4 Å above the surface, is attracted to the perfect surface with a force of several pN. This is just one of the many factors which cause contrast in the surface image in the attractive mode of observation. In reality the tips are constructed from ionic or semi-ionic materials such as silica, Si_3N_4 or oxidized silicon, which are protonated in humid air or in water. Therefore the tips are likely to consist of ions and inert groups such as silanol or bi-silanol [23]. Recently we have studied the interaction of an SiO molecular tip with the (001) MgO surface [24], and the more complex SiO_2 tip with a silanol group at its end with the (001) NaCl surface [8], using quantum-chemical techniques. These studies have revealed the complicated character of the tip–surface interaction and demonstrated the considerable surface distortion that occurs when the tip–surface separation becomes smaller than 2–3 Å.

In this paper we leave aside important issues concerning the details of the structure of liquid layers and their chemical interaction with tips and surfaces, and focus on the role of the chemical nature of the tip and the nano-asperity at its end, and the interaction of this nano-asperity with the surface at long and short distances, including surface penetration. We report the results of an extensive theoretical study of the interaction of three different types of tips, composed of SiO_2 and MgO, with the (001) surfaces of LiF, NaCl and CaO. We employed a new computer code MARVIN [25], based on the atomistic simulation technique, which we are currently developing as a routine tool for studies of surface processes including AFM. The aim of this study is to answer more clearly the following questions.

(i) What is the optimal tip–surface distance at which the tip will 'see' perfect or only slightly perturbed surfaces, and how does it depend on the chemical nature of the tip and the surface? How strong are the tip and surface distortions at small tip–surface distances and large applied forces?

(ii) Which kinds of point defects can be detected on ionic surfaces, and what are their expected images?

In section 2 the model of the tip–surface interaction used in our calculations is presented. In section 3 the calculation techniques are discussed. The results of our calculations are given in section 4, and the discussion and conclusions of this study are presented in section 5.

2. The model of the tip–surface interaction

We performed calculations for several models representing the end of the tips and their interaction with the (001) surfaces of LiF, NaCl and CaO. The chemical interaction of the liquid with the tip is taken into account via the specific microscopic structure of the very end of the tip, reflecting the possibility of its oxidation and protonation. Otherwise the liquid is considered to be inert and not contributing to the imaging. We assume that liquid molecules adjust their positions in response to the tip's excursions and deflections. In this simplified model, the role of the liquid is to provide an elastic lubricant which counterbalances the liquid–film meniscus forces and van der Waals forces due to the macroscopic size of the tip, and prevents the tip from penetrating the surface layer. Note that in this model the dielectric screening of the electrostatic interaction due to the liquid layer is also neglected. At large applied forces the tip can poke through the liquid layer and find itself inside the surface. Whether it is possible to obtain atomic resolution in this case is one of the questions which we try to address in this paper.

When all the forces acting at the cantilever at each particular scanning point are equilibrated, the actual position of the tip is determined by the thickness of the liquid layer (if any), the shape and chemical structure of the tip, and other factors. Thus, depending on the distance, the tip–surface 'chemical' interaction can be either repulsive, or attractive. Therefore our approach is first to calculate the related forces as a function of the chemical structure of the tip (SiO_2 or MgO), its shape, and its distance from the surface. These forces are the gradients of the adiabatic potential energy surfaces due to the interaction of the tip with the surface. In this context 'atomic resolution' means the difference in tip deflections at different surface atomic sites in variable-deflection mode, or at a certain force in constant-force mode. The dependence of this contrast on the tip position for different surfaces should give us an idea of the ideal 'resolution' of AFM and of the chemical identity of the ions at the surface.

Much more complicated issues concern the ability of AFM to resolve point defects, and the vertical and horizontal displacements of perfect surface ions and those around a point defect. The surface distortion induced by the tip is one of the important factors related to this problem. Another factor concerns the defect stability. In order to gain better understanding of these points we considered several plausible point defects which could be observed experimentally, i.e. Mg and O impurity defects near the (001) LiF surface, and the OH^- molecular ion substituting for Cl on the (001) surface of NaCl. Their stability, adiabatic barriers for diffusion, and AFM images were studied.

2.1. The tip

It is important to understand the strength of the chemical interaction between the tip and the surface ions, and whether it is possible to optimize the chemical structure, hardness, and shape of the tips in order to obtain better and more reliable images, or perhaps a degree of chemical specificity. Therefore, it is necessary to consider the atomic composition and structure of the tip, and the role of its chemical nature.

Si_3N_4 tips have been used in many recent studies with the Nanoscope II and have yielded good atomic images of alkali halides and of some alkali–earth fluorides [8,16]. In the study by Ohnesorge and Binnig [10], sensitive silicon cantilevers with ultra-sharp tips were employed for AFM imaging of the calcite cleavage plane. Since the surface of silicon oxidizes in air, it seems reasonable to assume that the outer layer of the tip is formed from SiO_2. According to [23], deposited Si_3N_4 usually contains a considerable amount of dissolved oxygen in the lattice and silanol Si–O–H groups in a surface film. Silanol groups also terminate typical SiO_2 surfaces in air [26,27]. Therefore, we consider a local structure corresponding to a silanol-terminated SiO_2 surface as the basis for the construction of an atomistic model for Si, SiO_2 and Si_3N_4 tips. One of the possible nano-structures of the end of the tip was suggested in our previous work [8]. It contains four silicon atoms and ten oxygen atoms (see figure 1). The central silicon atom of the cluster is fully coordinated by oxygen atoms, and all non-bridging oxygen atoms are terminated by hydrogens. In addition, the three remaining three-coordinated silicon atoms are also terminated by hydrogen atoms, as shown in figure 1. This tip model contains 24 ions, $Si_4O_{10}H_{10}$ (we will call it the SiOH tip in subsequent discussion). It is neutral and has seven silanol groups directed toward the sample surface. In order to make the tip 'sharp', one of the silanol groups is located closer to the surface than others.

To make our results more general with respect to tip shape, chemical structure, and hardness, we have studied MgO as an alternative material for the tip. More specifically, we considered a cube $Mg_{32}O_{32}$ oriented with its (111) axis perpendicular to the 'scanned' surface. The cube's corner makes a pyramid with an oxygen ion at its end (see figure 2).

This presents a model of an ionic tip which is much less 'sharp' than that with a silanol group at the end. The effective charge on the oxygen is $-2e$ (where e is the charge on a electron), contrasting with the charge on the hydrogen atom at the end of the silanol group, which is about $+0.4e$. This allows us to study in more detail the effects of the Coulomb interaction between the tip and the surface. Although MgO is quite a hard material, the local hardness of the corner, which we treat as a tip, is much less. Consideration of its interaction with different surfaces at various distances and applied forces will provide a useful insight into the problem of tip stability with respect to different surfaces.

It is known that water molecules can dissociate into H^+ and OH^- on MgO surfaces [28]. Protons bond strongly to the surface oxygen ions. For comparison with the results of calculations for the protonated SiO_2 tip interacting with the (001) NaCl surface, analogous calculations for the 'protonated' MgO tip were done (which we refer to as the MgOH tip in future discussion). Although in both cases the total charge of the tip was zero, there is an important difference between them. In SiO_2 the proton charge was compensated locally by the OH^- group attached to the nearest silicon ion. In the case of MgO, an OH^- group preserving the system neutrality was attached to the magnesium ion at the opposite corner of the cube. Therefore the end of the tip had a local charge of $+1$. This represents the situation where the presence of water or other liquid leads to formation of a charged tip [12,23].

3. Calculation techniques

We have focussed mainly on the calculation of an adiabatic potential energy surfaces (APES) and corresponding forces for the tip–surface interaction, and have not taken into account energy dissipation in the scanning process. The large number of relaxing ions requires a semi-empirical technique for energy calculation. We have, therefore, employed both a semi-empirical quantum-chemical method (CLUSTER code [29]), and an atomistic simulation technique (MARVIN code [25]).

3.1. Quantum-chemical method

The CLUSTER code has been described in several recent publications [29,30]. We will, therefore, focus our discussion only on the details which are essential for the present study. The program employs both the embedded molecular cluster (EMC) model [31] and the periodic large unit cell (LUC) method [32] and is based on the intermediate neglect of differential overlap (INDO) approximation of the unrestricted Hartree–Fock–Roothaan method [33]. It allows us to determine the electronic structure of a quantum mechanically described cluster that contains several tens of ions. It employs a minimal valence Slater basis set and uses a single-determinantal approximation for the wavefunction and therefore does not take into account van der Waals interactions. The lattice relaxation in the present study includes only ionic displacements from the lattice sites.

The calculation scheme of the CLUSTER code and the parameterization of the INDO method are described in [29]. The EMC model was employed in all the present calculations. The crystal surface was simulated by a $Na_{25}Cl_{25}$ molecular cluster comprising two planes of 25 ions embedded in the slab of five lattice planes (see figure 1). The tip structure was optimized separately using the CLUSTER code. The Si–O–H angle within the central silanol group was found to be 120 degrees. However, in order to simplify the model we made it 180 degrees and did not vary this angle in further calculations. Although this makes the tip stiffer, we believe that this does not affect our qualitative conclusions.

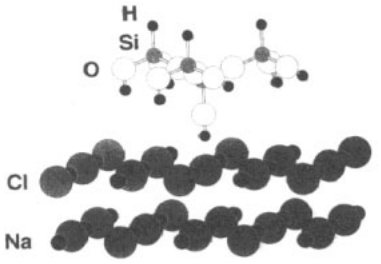

Figure 1. Diagram of the SiOH tip and (100) NaCl cluster treated explicitly in the CLUSTER calculations. This ensemble is embedded in an infinite five layer slab of NaCl which is not shown in the figure.

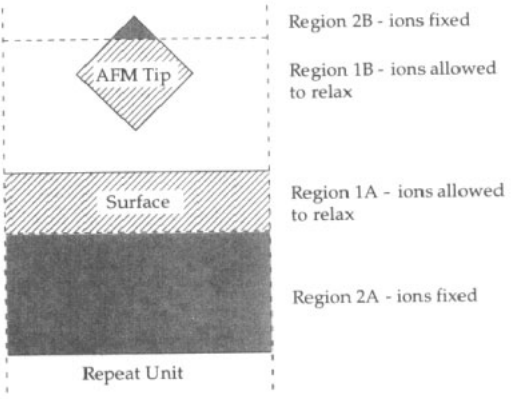

Figure 2. Schematic of the repeat unit for the tip and surface used in the MARVIN atomistic simulations (see also figure 7).

3.2. MARVIN atomistic simulation technique

The atomistic simulations presented in this work have been performed by a new surface code MARVIN [25]. This program adopts a many block approach, with planar two-dimensional periodic boundary conditions parallel to the interface. Each block consists of two regions as shown in figure 2. The first contains the ions which are relaxed explicitly until there is zero force on each of them, while the ions in the second are fixed. Thus, the model of a surface consists of a block (A) with its region 1 containing the ions closest to the surface, and the ions in region 2 are fixed to represent the electrostatic potential of the remaining lattice (see figure 2). The methodology is closely related to that used by Tasker [34] in the MIDAS code, but MARVIN is considerably more flexible as regards the interatomic potentials that may be used and the complexity of the systems that may be studied. In the atomic force microscope calculations, the tip is placed in a second block (B), with its region 1 containing most of the ions which interact with the surface, and the few remaining ions placed in region 2 to fix the shape and position of the tip. Each block has its own attributes, such as the type of potentials used to describe it. The advantages of adopting a many block approach will become apparent in future work, where the effects of water or the imaging of a molecule adsorbed on a surface will be examined. Clearly these new interactions will be molecular in nature and will need to be treated by molecular mechanics potentials, rather than the ionic model used here to describe the tip and surface and their interaction.

The code in its present version employs periodic boundary conditions, which has advantages for studies of perfect surfaces, interfaces and periodic adsorption. However, this confines the simulation of the AFM to a periodic array of tips which interact with each other. To minimize this interaction, the simulation box needs to be as large as possible. Increasing the number of ions, n, in the simulation slows down the program execution appreciably as the calculation time is order n^2. To minimize this problem, we have incorporated the idea of 'freezing' into the calculations. This involves taking an ion out of the minimization if the force on it is less than a given value. There is no guarantee that the force on this ion will not increase as the rest of the ions relax around it, and this is checked for at the end of each calculation. This technique has been found to be extremely effective for the AFM calculations presented here.

The functional forms of the potentials used to describe the tip and surface and their interaction are based on an ionic model [35]. The major interaction is between charges centred on the ionic positions of the ions, with electronic polarization incorporated via the Dick–Overhauser shell model [36]. These Coulomb interactions are very long-range and so the crystal sums converge very slowly. Hence a two dimensional Ewald summation technique has been employed [37]. In this work, two-body potentials were used to represent the non-Coulombic interactions between the ions, although the program can handle three- and four-body potentials to describe covalent interactions. The range over which these non-Coulombic interactions operate is determined by a potential cut-off. We note that the code has the facility to use a molecular mechanics formalism, where the connectivity of a molecule is used to determine the appropriate form of interaction for each potential.

Table 1. Short-range potentials[a] used.

Between ions	Potential type	A or D	ρ or β	C or r_0	source
O–O	Buckingham	9574.96	0.2192	32.0	This work
Li–O	Born–Mayer	828.01	0.2793	—	This work
Na–O	Born–Mayer	1677.83	0.2934	—	This work
Mg–O	Born–Mayer	1284.38	0.2997	—	This work
Ca–O	Born–Mayer	1219.24	0.3376	—	This work
F–O	Buckingham	464.55	0.3363	22.1	This work
Cl–O	Buckingham	4393.1	0.2721	62.2	This work
F–F	Buckingham	911.69	0.2707	13.8	This work
Li–F	Born-Mayer	443.84	0.2714	—	This work
Na–F	Born-Mayer	1459.76	0.2605	—	This work
Mg–F	Buckingham	2902.29	0.23668	1.866	Reference [38]
Cl–Cl	Buckingham	2021.3	0.3588	88.98	This work
Na–Cl	Buckingham	3046.4	0.2836	12.82	This work
Mg–Cl	Buckingham	2511.51	0.2857	6.22	This work
Na–Na	Buckingham	6927.8	0.1836	4.43	This work
Na–Mg	Buckingham	28261.4	0.1510	2.10	This work
O_t[b]–H	Morse	7.0525	2.1986	0.9485	Reference [39]
Na–H	Born–Mayer	83.09	0.2946	2.10	Reference [40]
Cl–H	General[c]	1851.0	0.2014	1.565	This work

[a] The potentials given above have the functional form: $W(r) = A\exp(-r/\rho)$ (Born-Mayer); $W(r) = A\exp(-r/\rho) + C/r^6$ (Buckingham); $W(r) = \{1 - \exp[-\beta(r - r_0)]\}^2 - D$ (Morse).

[b] O_t is the oxygen ion of the OH group at the end of the MgOH tip. It was treated as non-polarizable with the effective charge equal to $-1.4263e$. The effective charge of the H ion was $0.4263e$ [T2]. The parameters of the short range interaction between the O_t ion and Mg, O, Na, and Cl ions of the tip and the surface were the same as those for the O ion. The only difference was in the Coulomb interaction. Only the Coulomb interaction between the H and Mg ions was taken into account.

[c] This interaction was best fitted to the pair potential which had an additional D/r^4 term with $D = 7.574$.

The parameters of the pair potentials used in this work are summarized in table 1. The short-range potentials for most of the ions were specially optimized. The aim of this optimization was to maintain the consistency between the different interactions and to reproduce the characteristics of the perfect lattices correctly but still produce a potential whose functional form is robust with respect to significant distortions in the bond lengths away from equilibrium values. In particular, the oxygen–oxygen potential was determined by simultaneously fitting the short range parameters to reproduce the lattice parameters of a range of different binary and ternary oxides. All other potentials were initially derived using an electron-gas method and further refined by fitting to the perfect lattice properties

of the appropriate materials, i.e. for MgO, NaCl, LiF, MgF_2, Li_2O, Na_2O. In cases where no lattice data were available, to aid the fitting procedure an empiricizing method was employed [41] which uses the differences in potentials derived using an electron-gas method and an appropriate empirical potential (e.g. electron-gas F–O and F–F; empirical F–F). For anion–anion potentials, the C_6 dispersion terms were determined using the Kirkwood–Slater formulae [42]. Only Coulomb repulsion was taken into account for Li–Li and Mg–Mg interactions. All the ions, except O_t and H, had their full formal charges. Only anions O, F and Cl were polarizable. Their shell model parameters [35,36] were the following: $Y_O = -2.04e$; $K_O = 6.3$; $Y_F = -1.3776e$; $K_F = 24.26$; $Y_{Cl} = -1.984e$; $K_{Cl} = 13.209$.

To derive the short-range potential between the hydrogen ion of the Ot–H group at the end of the MgOH tip and the chlorine ion at the surface we used the following procedure. The interaction of the $Mg_{32}O_{32}H^+$ tip with the individual Cl^- ion was calculated both quantum-chemically and using the MARVIN code in a wide range of separations. In the latter case only the Coulomb interaction between the hydrogen and chlorine was included. Then the results of both calculations were subtracted, and the difference was fitted to a pair potential.

Using the MARVIN code and this set of parameters we calculated the reconstructions of the perfect (001) surfaces of LiF, NaCl and CaO. The results are qualitatively similar for all three crystals: the cations displace slightly inward and the anions outward from the crystal perpendicular to the ideal surface plane. The magnitudes of these displacements are about $0.01a$ (a is the bulk interionic separation) for LiF and CaO, and about $0.02a$ for NaCl. A very similar surface relaxation was calculated for NaCl using the CLUSTER code. We note in passing that the geometry of the relaxed $Mg_{32}O_{32}$ cluster is not in fact cubic, but rather rectangular with rounded corners. It compares well with that calculated in previous studies [43].

In all the MARVIN calculations of the tip interacting with the perfect surfaces, the surface region 1 contained two planes of 72 ions, which were allowed to relax. In the defect studies region 1 contained four crystal planes of the same size. Region 2 typically contained five planes of frozen ions. In all the calculations, the region 1 of the MgO tip contained 44 of the 64 ions comprising it.

4. Results of calculations

We consider our model as one which represents a quite common situation when there is an oxygen ion or a chemical group such as silanol at the end of the tip, and focus our attention first of all on qualitative features of the mechanisms of atomic imaging using AFM. We explored, therefore, only one of the possible orientations of the SiOH, MgO and MgOH tips relative to the surface. These orientations were chosen arbitrarily, and then kept the same in all the calculations. In most cases the calculations were made for the tip moving down perpendicular to the surface above different surface points (cation and anion sites, and some intermediate positions) until it penetrated the surface to a certain extent, after which we moved the tip back up. Calculations were also made for the tip moving inside the crystal parallel to the surface plane. In the MARVIN calculations the total energy of both regions 1 was minimized with respect to the positions of the cores and shells of the relaxing ions (see figure 2) at each position of the tip. In the CLUSTER calculations only the O and H atoms of the silanol group at the end of the tip and all the atoms inside the quantum cluster on the surface were allowed to relax to new equilibrium positions. The forces acting between the tip and the surface were calculated as the first derivatives of the APES with respect to the shift of the frozen part of the tip along the z axis.

Four sets of calculations were performed. The quantum-chemical CLUSTER calculations were made for the (001) NaCl surface and the SiO_2 tip. For the sake of comparison analogous MARVIN calculations were performed for this surface using the MgOH tip. The interaction with the LiF and CaO (001) surfaces were studied only for the MgO tip using the MARVIN code.

4.1. General trends

The APES corresponding to the tip moving down towards the surface above cation sites for the four cases are presented in figure 3. The values on the x axis are the displacements of the frozen part of the tip, d, relative to the frozen part of the surface from the initial configuration of the system. For convenience they are calculated in such a way that the far right point corresponds to the initial distance between the end of the tip and the perfect surface plane, whereas 0 corresponds to the situation where the last ion of the *unrelaxed* tip would cross the perfect surface plane. Note that due to the tip and surface relaxation this 'crossing' is only imaginary. However, for convenience of discussion we will further call d a tip–surface distance.

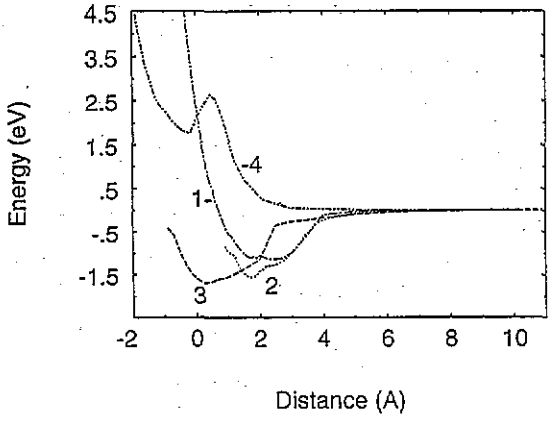

Figure 3. Energy versus distance curves for the different tips above a cation site. (1) MgO tip above LiF surface; (2) MgO tip above CaO surface; (3) MgOH tip above NaCl surface; (4) SiOH tip above NaCl surface.

Despite differing in shape, the APES can be clearly divided into three regions. In the first region, in which d varies from 10 Å to about 4.0 Å, the tip–surface interaction is relatively weak. In the second region, which usually corresponds to the values of d less then 3.5 Å, strong chemical interaction between the tip and the surface ions takes place, and the APES sometimes have a quite irregular shape. Finally, in the third region the strong repulsion between the tip and the surface takes place. Let us now consider these three regions in more detail.

4.1.1. Large tip–surface distances. There are three main contributions to the tip–surface interaction at large distances in our model: (i) the van der Waals interaction; (ii) the interaction of the tip ions with the electric field produced by the surface and vice versa; (iii) the polarization interaction, i.e. the interaction of the dipole moments induced on the tip ions with the surface electric field and those on the surface ions with the tip electric field, and the interaction between the dipoles themselves.

The van der Waals attraction is taken into account via the C_6 dispersion terms in the pair potentials. Note that the sum of these interactions is taken over all ions in regions 1 and 2

of the blocks A and B (see figure 2). It should be proportional [12] to $1/d^3$ if the tip radius R is smaller than d, and to $1/d$ for $R \gg d$. The van der Waals interaction is long-range and does not depend on the tip lateral position at large tip–surface distances. This effect depends on the tip's shape. For the MgO tip used in this work, the lateral dependence of the van der Waals interaction becomes significant when the distance between the surface and the end of the tip is less than about 2.5 Å.

The electric field produced by the neutral (001) surface of the FCC lattice is periodic and decays exponentially [44] with the distance from the surface plane, z. At large distances, such as 2–3a it behaves as $\exp(-kz)$, where $k = \pi/a$ (1.1–1.6 for our surfaces). At closer distances the contribution of other reciprocal lattice vectors becomes significant and the functional form of the surface electric field may include several exponents. This is also true for the neutral tip. However, because of its sharp form, the electric field produced by the tip decays much more slowly. For instance, for the MgOH tip in the direction perpendicular to the surface it behaves approximately like $\exp(-0.25r)$, where r is the distance from the H atom. Therefore both electrostatic terms of the tip–surface interaction should increase exponentially as the tip approaches the surface.

There are two sorts of dipoles induced on the surface and tip ions. All the perfect surface ions initially bear small dipole moments due to the gradient of the crystalline potential near the surface and its rumpling. The electric field produced by the periodic lattice of these dipoles decays exponentially with the distance from the surface [12]. The tip ions are also initially polarized due to its shape. As the tip approaches the surface, polarization of the surface ions increases and some of them strongly displace from their initial positions. The dipole–dipole interaction between the most polarized surface ions and those of the tip is approximately proportional to $1/d^6$, although it may behave in a more complicated way at small tip–surface distances where a large number of ions may be polarized.

First, let us consider the interaction of the MgO tip with the (001) surfaces of LiF and CaO. The calculated force versus distance curves are presented in figure 4. For LiF, these curves practically coincide between 7 and 11 Å for all lateral tip positions studied (i.e. above anion and cation surface sites, as well as above the intermediate position midway between cation and anion). The APES can be well fitted by the functional form $E(d) = \mathrm{A}/d^3 + \mathrm{B}/d$, where A is much larger than B. These two factors demonstrate the van der Waals nature of this interaction. The electrostatic interaction, which becomes significant at distances smaller than 7 Å, splits the APES and the force curves and makes an exponential contribution to the functional form of the interaction. The electric field produced by the surface of CaO decays slower than that for LiF because of the difference in the ionic charges and the lattice constants. In fact in CaO, the electrostatic contribution to the interaction is larger than that of the van der Waals interaction even at large distances. The gradient of the electric field is larger at the last oxygen ion than at upper tip ions. This determines the qualitative character of the interaction: repulsion above anion sites and attraction above cation sites (see figure 4).

The force curves representing the interaction of the MgOH tip with the (001) NaCl surface look qualitatively very similar to that of MgO with LiF (see figures 4 and 5). However, the magnitudes of the interaction and forces are approximately twice as large in the case of NaCl. This results from the fact that the dispersion interaction between O and Cl ions is much larger than that between O and F (see table 1), and from the difference in the electrostatic contributions. The latter is caused by the non-compensated positive charge at the end of the MgOH tip. At relatively small tip–surface distances (less than 4 Å) the repulsion of the positively charged tip from the cation site and its attraction to the anion site split the curves. This effect is much more pronounced for SiOH and NaCl.

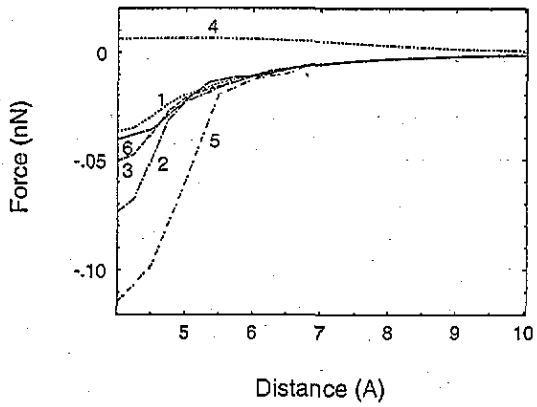

Figure 4. Force versus distance curves for a MgO tip above (100) surfaces of LiF and CaO at large separations. Positive forces correspond to repulsion. Curves (1)-(3) correspond to LiF and (4)-(6) to CaO. (1) and (4) are above anion sites; (2) and (5) are above cation sites; (3) and (6) are above sites equidistant from a cation and anion along the (100) axis.

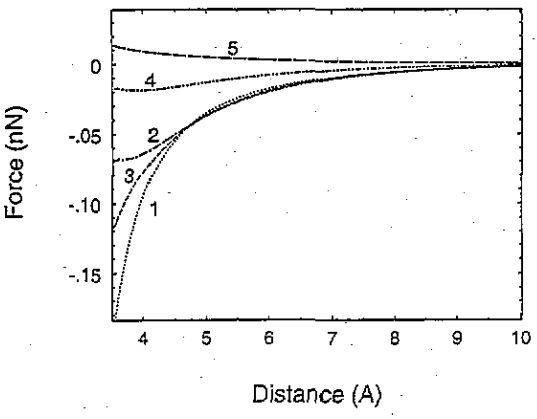

Figure 5. Force versus distance curves for MgOH and SiOH tips above the (100) surface of NaCl at large separations. Curves (1)-(3) correspond to the MgOH tip and (4)-(5) correspond to the SiOH tip.(1) and (4) are above anion sites; (2) and (5) are above cation sites; (3) is above the site equidistant from a cation and anion along the (100) axis of NaCl.

The quantum-chemical calculations on the interactions between the SiOH tip and the (001) surface of NaCl do not take into account van der Waals interactions. Therefore when the massive part of the tip is relatively far from the surface, the tip–surface interaction is determined mainly by the electrostatic interaction between the polarized O–H group at its end and the surface ions. It becomes virtually negligible at about 4.5 Å. For distance 1 Å $\leqslant d \leqslant$ 4.5 Å above the surface, there is a repulsion above cation sites and an attraction above anion sites. Stronger repulsion above cation sites is caused by the electrostatic repulsion between the two positively charged species: cation and hydrogen. Above anions the attraction between the hydrogen and chloride is partly compensated at large distances by the repulsive force between the oxygen and chlorine ions. Another important factor is the attraction between the oxygen ion and the nearest cations surrounding the anion site. Note that similar effects occur for all the cases considered.

The magnitudes of the forces acting between the tips and the surfaces increase from 0 to about 30–60 pN at $d \sim$ 3–4 Å (see figures 4 and 5). In this range the surface distortion induced by the tips is quite small and the displacements of ions from their sites do not typically exceed $0.02a$. Note, that although we consider the tip moving up and down above the certain surface points, a small and reversible surface distortion allows us, in principle, to reconstruct the whole image, and to relate our results with the 'real' scanning process, where the tip moves *along* the surface. This corresponds to the intuitive understanding of an ideal scanning as a process in which the surface and the tip do not distort irreversibly and images are reproducible. However, in real experiments the amplitude of the tip's deflections

above different surface sites depends not only on the forces discussed above, but also on the structure and elasticity of the liquid layer. Therefore the amplitudes obtained in these calculations (say, about 0.5 Å for the force 40 pN in the case of the MgO tip and the LiF surface) demonstrate only the scale of possible deflections. The situation changes at smaller distances, where the separation between the tip and the surface becomes close enough for chemical bonding.

4.1.2. Chemical bonding. As the tip approaches the surface, several different situations can be expected which depend on the geometry, chemical structure and local hardness of both materials. (i) If the hardness of the microasperity of the tip is stronger than that of the local surface area it may penetrate the surface and produce severe surface damage. In the opposite case the tip itself may be considerably damaged. (ii) The tip may adsorb atoms from the surface if their chemical bonding to the tip atoms is larger than to the surface. This may lead to hysteresis in the APES and force curves as the tip moves up and down during scanning. (iii) Both these effects depend on the tip's shape and orientation. In the area of strong tip–surface contact the number of possible variants and atomic configurations increases dramatically. Therefore the calculations are able to demonstrate only qualitative trends and to give some models. The qualitative results of this study may be summarized as follows.

(i) All three tips considered in our study (MgO, MgOH and SiOH) are harder than the surfaces of alkali halides. Therefore, despite considerable distortion of their structure, they easily penetrate the surfaces of LiF and NaCl. That does not happen, however, in the case of CaO, where the MgO tip effectively 'breaks' when approaching the surface at the distance about the lattice constant of CaO (2.405 Å) both above cation and anion sites. In fact the oxygen ion at the end of the tip displaces inside the tip, which is destroyed due to the strong repulsion from the surface ions (see figure 6).

(ii) The surface deformation by different tips has common features characteristic of certain tip–surface separations. They are illustrated in figure 7 for the MgOH tip approaching the (001) NaCl surface. At relatively large distances (more than 2.5 Å) the surface deformation is small and elastic (figure 7(*a*)). At some stage (in our case when d = 2.5 Å) the hydrogen ion starts to pull the Cl ion out from the surface (figure 7(*b*)). The same happens above a cation site but at smaller d (see the sudden drop in energy in figure 3). This effect is characteristic of all cases considered. At smaller distances the tip repels the ions inside the surface first producing elastic deformation over a large surface area. When the tip–surface distance becomes smaller than about 1 Å, a defect forms when the surface ion closest to the tip displaces into the interstitial position. At this distance other tip atoms come close enough to the surface to pull some ions out of the surface (figure 7(*c*)). Finally, when the tip penetrates the surface, several surface ions displace into interstitial positions and some of them adsorb onto the tip (figure 7(*d*)). This surface deformation is not reversible and leads to the hysteresis in the APES if the tip moves back to its initial position.

4.1.3. Repulsion and hysteresis. When the massive part of the tip approaches the surface, it is repelled strongly as can be clearly seen on all the APES presented in figure 3. This repulsion corresponds to the surface indentation. It may be also accompanied by an effective change of the tip's shape as many of the surface ions adsorb on its surface. The latter strongly depends on the chemical structure of the tip and the surface. In our calculations, which correspond to 'molecular' dimensions, it is trivially determined by the ratio between binding energies of the ions at the initial surface and those at the tip. The difference can be readily seen if we compare the SiOH tip, 'covered' with the silanol groups, and the MgO tip.

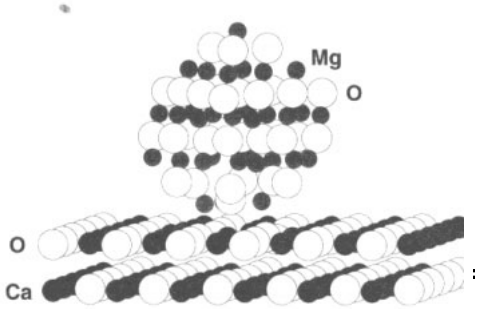

Figure 6. Diagram of a MgO tip breaking when pressed into the (100) surface of CaO with a force of about 1 nN at a distance of 2 Å from the surface. Note the small deformation of the surface.

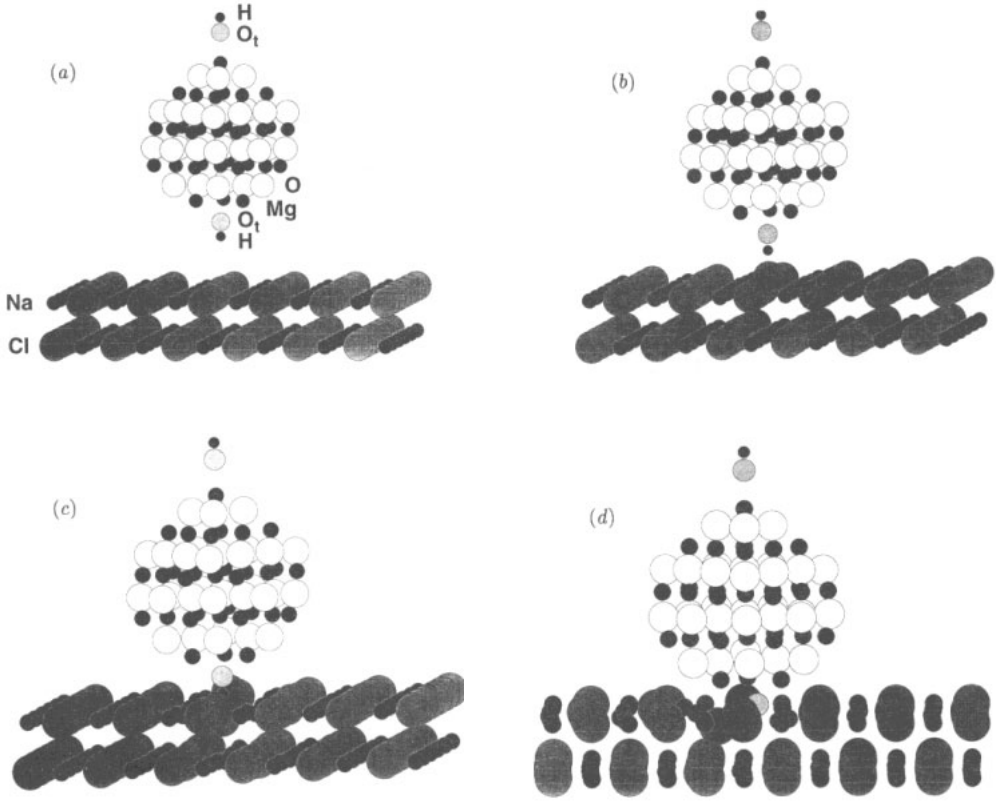

Figure 7. Progress of the MgOH tip descending into the (100) surface of NaCl above an anion site. Both regions 1 and 2 of the tip are shown but only the region 1 of the surface. Note the O_tH group at the top of the tip to make the system neutral. (a) d = 4 Å. The surface and tip are only slightly perturbed. (b) d = 2.5 Å. The anion is displaced outwards from the surface towards the approaching tip. The tip is still intact. (c) d = 0.7 Å. The surface is strongly perturbed with the anion now displaced inside the surface. (d) d = -0.4 Å. Both the tip and surface are greatly distorted. The tip has entered the surface and displaced the anion into the interstitial position.

Although there is a chemical interaction between the hydrogens of the tip and the chlorine ions at the surface of NaCl (see discussion in [8]), the energy of this interaction is much less than that necessary to produce an anion vacancy on the surface (about 7 eV [11]).

Therefore, this interaction leads to reversible surface distortion. However, the binding of the Li and F ions to the surface of MgO is larger than the defect formation energy at the surface of LiF. Several ions adsorb on the grains of the MgO tip. This can be best seen in figure 8(*a*) showing the tip penetrating the surface of LiF above an anion site.

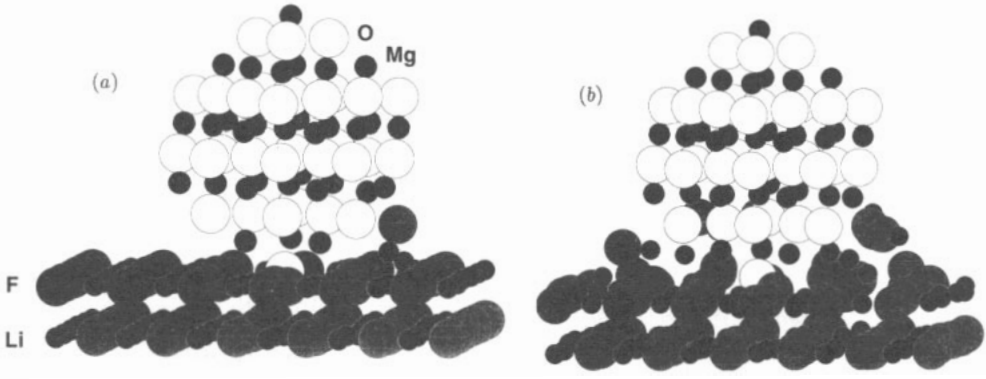

Figure 8. MgO tip absorbing ions as it scans the surface of LiF. (a) tip penetrating the surface above anion site. (b) tip displaced towards cation site and up out of the surface by 1 Å. The beginning of the formation of a 'neck' can be clearly seen.

If we now simulate a scanning process and move the tip in the direction of the cation site, the surface deformation becomes even larger. In this situation the tip works like a plough, moving several ions along with it. The beginning of the formation of a 'neck' between the tip and the surface can be clearly seen in figure 8(*b*), corresponding to the tip position between cation and anion sites and about 1 Å above the surface. Similar effects have been studied experimentally [45] and theoretically [21] for metallic surfaces.

We note that the effects of hysteresis are closely related to adhesion and wear of the tip and the surface materials, and should be described in terms of surface free energy and simulated using molecular dynamics. Presently this technique is too time-consuming for ionic surfaces due to the two-dimensional crystalline sums which need to be computed at each time step. However, we believe that the qualitative effect is clearly demonstrated.

4.2. Surface defects

Imaging of atomic scale surface defects is the most convincing way of demonstrating true atomic resolution. Step edges have been observed on several surfaces with atomic resolution [8,10]. Some point defect candidates, imaged as missing lattice ions, have also been reported recently [8,11]. Since the time required to raster an atomic width in many AFMs is not much smaller than 0.1 s, only very stable defects can remain in the observation area during scanning and thus be imaged. Defect diffusion may be stimulated by their interaction with the tip. Amongst the many other factors which can make observation of point defects so rare is their relatively low total concentration in the sample, and, in particular, in the first surface layer. In this section we report the results on the stability and mobility of several types of defects near surfaces of LiF and NaCl, and their interaction with the AFM tip.

One can consider at least three sources of point defects near the surfaces of ionic crystals. These can be Schottky pairs of cation and anion vacancies (the formation energies of these

defects are about 2.7 and 2.5 eV in LiF and NaCl, respectively), impurities, and defects produced during AFM scanning. In this paper we have studied two well known impurity defects which are common in LiF samples: Mg^{2+} substituting Li, and O^{2-} substituting F in their regular sites. Their excess charges are compensated by cation and anion vacancies respectively, which are localized at the nearest-neighbour position. We have also studied the OH^- ion in an anion vacancy on the surface of NaCl. Anion vacancies thermally generated near the surface can trap the OH^- ions from the adsorbed water or from solution. Vacancies can also be produced during scanning, as was demonstrated in the previous section.

4.2.1. Defect structure and stability. Properties of these defects in the bulk were calculated in previous studies using similar techniques [46]. Therefore we focused our attention on their structure near surfaces. The impurity-vacancy dipoles in three surface planes were calculated using the MARVIN code. Four surface planes were included in region 1 (see figure 2) and each contained 72 ions. The periodically translated dipoles interact with each other. There is, therefore, a technical question as to how large the repeat unit needs to be to eliminate the influence of this interaction on the defect structure and their diffusion adiabatic barriers. Comparative calculations for units of various sizes have demonstrated that our unit is large enough for this purpose. The relative energies of various dipole configurations considered in this work are summarized in table 2. One can see that the configuration where the vacancy is in the surface layer and the impurity ion is in the next layer is preferable for both the Mg^{2+}–V_c and the O^{2-}–V_a dipoles, although this is less pronounced for the oxygen dipole. This is mainly the result of the difference in the crystalline potential in the surface layers and surface polarization. In particular, the magnitudes of the Madelung potential in the non-relaxed surface layer and in the two next layers are 1.6816, 1.7483 and 1.7476, respectively.

Table 2. The calculated energies (in eV) for the different configurations of Mg^{2+}–V_c and O^{2-}–V_a dipoles near the (001) surface of LiF. Integers in the first and in the second columns indicate the number of the plane where the vacancy and the impurity are located. 0 corresponds to the surface plane.

Impurity	Vacancy	Mg^{2+}–V_c	O^{2-}–V_a
0	0	0.28	0.02
1	0	0.00	0.00
0	1	0.40	0.21
1	1	0.11	0.16
2	1	0.15	0.17
1	2	0.21	0.18
2	2	0.20	0.18

The displacements of the ions surrounding the defects are very close to those obtained in the bulk [46], therefore, we do not present them here. However, since the displacements of ions near the cation vacancy on the LiF surface are of some interest from the point of view of their possible observation by AFM, they are discussed in the next section.

The OH^- ion substituting Cl^- on the surface of NaCl was studied using the quantum-chemical CLUSTER code. However, for the sake of comparison and in order to test our pair potentials we performed the calculations of this defect using the MARVIN code too. The atomic structures obtained by both techniques are very similar. The OH^- ion is oriented perpendicular to the surface plane with its O ion located almost in the centre of the vacancy

and the H ion directed out of the surface. The five nearest-neighbour cations are displaced by $0.08a$ towards the O ion. Similar calculations performed for the bulk defect using the CLUSTER code gave the (100) orientation of the molecular ion, which is well known from experimental studies [47]. Hardly surprisingly the OH^- ion is very stable in the anion vacancy. In particular, the lowest energy for the OH^- adsorbed on the surface near the anion vacancy is about 3.3 eV higher than that inside the vacancy.

4.2.2. Adiabatic barriers for defect diffusion. In order to characterize the mobility of the defects the adiabatic barriers for their diffusion were first calculated. Preference was given to the most stable defect configurations at the surface as this is relevant to this study. Let us first consider the Mg^{2+}–V_c dipole. The barrier for the cation vacancy jumps on the surface around the Mg^{2+} ion located in the next surface plane was calculated to be 0.36 eV. The barrier for the Mg^{2+} jump into this vacancy is about 1.1 eV. If the dipole is located in the surface plane the latter barrier is found to be 1.3 eV. Very similar values were obtained also in the case of the O^{2-}–V_a dipole. In particular, the barrier for the O^{2-} jump from the second plane into the vacancy on the surface is about 1.0 eV, and that for the dipole located in the surface plane is about 1.1 eV.

The barrier for the anion vacancy diffusion on the surface of NaCl calculated using the CLUSTER code is 0.75 eV. Although these calculations do not include the effect of electronic polarization of the surrounding lattice, it is close to the experimental values (0.77–1.6 eV), and the results of previous calculations (0.72 eV) for the bulk material (see [48] for a discussion). The barrier for the OH^- ion to exchange places with the nearest Cl ion on the surface is 3.5 eV. However, the barrier for the OH^- ion jump into the nearest anion vacancy is much smaller and equal to 0.38 eV. So, as usual, the vacancy mechanism is much more effective. However, it requires the anion vacancy to have been generated and diffused to the vicinity of the OH^-.

These results qualitatively agree with the results of recent studies of the Mg^{2+}–V_c dipole diffusion in the bulk of Li_2O [49] and previous Mott–Littleton calculations on alkali halides [48]. Essentially vacancies are much more mobile than charged impurities and the mobility of the dipole is determined by the barrier for the impurity jump. This is the result of the interaction of the charged impurity with the crystalline field. It is interesting to note that, due to the same reason, the barrier points for Mg^{2+} and O^{2-} jumps between the two vacancies on the surface are located about $0.1a$ below the surface plane, i.e. 'inside' the crystal. Whereas the barrier point for the host cation jump between the two vacancies is located about $0.3a$ above the surface plane.

Accurate calculations of the jump rates would be certainly a matter of a separate study, especially because the saddle point vibrational frequencies may differ strongly from those in the initial and final states (see [50] for a discussion). However, applying Vineyard theory [51,50] in its simplest form and using as pre-exponential factors the maximum lattice frequencies ($12.6 \cdot 10^{13}$ s^{-1} and $5.1 \cdot 10^{13}$ s^{-1} for LiF and NaCl, respectively [52]) we feel safe to conclude that at room temperature the impurities will be localized in their sites for more than one hour. Experimental studies of thermoluminescence, optical absorption and ionic thermocurrents of magnesium-doped LiF samples [53] have demonstrated that the Mg^{2+}–V_c dipoles become mobile and begin to aggregate only at the temperatures higher than 100 °C. This is in good agreement with our estimates. However, the compensating vacancies can make several million jumps per second around the impurity at this temperature. A more complicated situation is the anion vacancy migration on the surface of NaCl. The calculated barrier for these processes is about 0.7 eV and simple estimates predict that one jump can happen each 0.1–1 s.

These values for jump frequencies can change by an order of magnitude due to compensation effects [50], and even more due to dissolution of the surface layer and interaction with the tip. However, we believe that impurities like Mg^{2+} or OH^- could be observed on these surfaces by AFM. It is worth noting, however, that the defects considered, although well known in the bulk, may have different forms near surfaces. In particular, charge compensation of Mg^{2+} or O^{2-} can take place by interstitial host ions that have been rejected to the surface on forming Schottky pairs instead of vacancies. In the next section we focus only on two representative defects: the cation vacancy and the Mg^{2+} ion on the (001) LiF surface.

4.2.3. Defect images by AFM. Amongst the many questions which can be asked regarding the possibility of imaging and identifying point defects on surfaces by AFM, we will address in a qualitative manner the following.

(i) Is it possible to distinguish a charged defect on the surface by AFM and perhaps even achieve a certain degree of chemical specificity?

(ii) Is it possible to resolve displacements of the ions nearest to the defect relative to their lattice sites?

(iii) How can the tip–defect interaction influence the results, and what might be the optimal conditions for observation?

As is already clear, at small distances the tip–surface interaction may considerably disturb the surface structure, therefore the calculations were performed only up to $d = 2$ Å. Two cases were considered: (i) the most stable configuration of the Mg^{2+}–V_c dipole with the cation vacancy on the surface and the Mg^{2+} ion in the second surface layer, and (ii) the Mg^{2+}–V_c dipole in the surface layer. The anions nearest to the vacancy are displaced into the surface plane by about 0.15 Å. The APES corresponding to the MgO tip approaching the LiF surface above the cation vacancy, the Mg^{2+} ion on the surface, the site position of one of the anions nearest to the vacancy, the real displaced position of this anion, and the intermediate position between this anion and the centre of the vacancy are presented in figure 9(*a*). Two characteristic features can be clearly seen. First, there is a considerable difference in the behaviour of the tip–surface interaction above the vacancy, the Mg^{2+} ion, and the three other positions. Secondly, at distances of about 3–3.5 Å from the surface, the tip starts to pull some of the ions out of the surface (in the Mg^{2+} case it is the magnesium ion itself), resulting in a considerable drop in energy. Thus the regime of a small perturbation in our model is limited up to the tip being about 4 Å from the surface plane.

The corresponding force versus distance curves in the range of d from 10 Å to 4 Å are presented in figure 9(*b*). (The curve for the tip above the regular anion site is added for comparison.) They demonstrate an average repulsion of the tip above the vacancy, a strong attraction to the Mg^{2+} ion, and very similar behaviour above the anion site and the displaced anion. The striking difference between the vacancy and the Mg^{2+} ion results from the Coulomb interaction of the tip with these oppositely charged defects. However, this interaction decays very rapidly as the tip shifts closer to the host ion sites. As a consequence of this, both defects can be seen with a good 'resolution', especially in the variable-deflection mode. This result also suggests that one of the possible ways to search for this type of defect is to make scans far from the surface where the tip–surface interaction is still small enough to obtain good atomically resolved images (at 5–6 Å, say).

Another point concerns the possibility of observing the displacement of the ion from the lattice site. This seems to be much more difficult. In particular, the difference between the force above the regular anion site and that above the centre of the displaced anion is

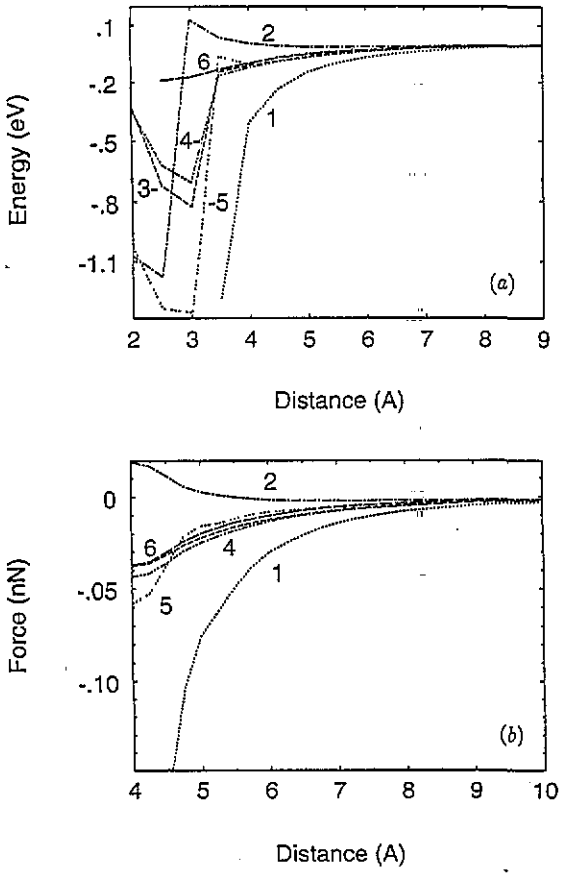

Figure 9. (a) Energy versus distance curves and (b) force versus distance curves for a MgO tip above the perfect and defective (100) surfaces of LiF. The latter is at large separations only. (1) above the Mg^{2+} ion substituting for the Li ion on the surface; (2) above the cation vacancy; (3) above the regular site position of one of the anions nearest to the vacancy; (4) above the real displaced position of that anion; (5) above the intermediate position between the displaced anion and the cation vacancy; (6) above an anion on the perfect (100) surface.

only about 4 pN when the tip is 4.5 Å above the surface plane. This is on the limit of even the best observed sensitivity. In the constant-force mode of about 30 pN the difference between the tip's deflections would be about 0.3 Å above these two points, which is close to the limits of thermal noise. Note that at distances closer than 4 Å, the interaction of the tip with the defect causes displacements of the impurity and the surrounding ions which are comparable or even larger than the difference in the tip's deflections. This is clearly seen in figure 10.

5. Discussion

What can these results tell us about experimental surface images? The general trends common for the cases considered may be summarized as follows.

The best conditions for 'atomic resolution' exist when the tip scans the surface at a distance of about 3–5 Å from the surface. This may correspond to the presence of one or two liquid layers between the tip and the surface. In this distance range the distortion of the perfect surface structure is still small enough for non-destructive imaging, whereas the tip–surface interaction is already large enough to observe good contrasts with existing cantilevers. Note also that less damaged surfaces are less soluble too. Scanning on large distances seems to be the necessary condition for observation of point defects with atomic resolution.

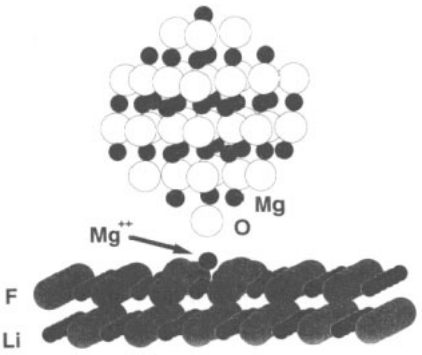

Figure 10. MgO tip above the Mg^{2+} ion substituting for Li on the (100) surface of LiF. Note that the displacement of the impurity towards the tip is greater than the displacements of the surface ions caused by the defect itself.

The electrostatic contribution to the tip–surface interaction makes a basis for 'atomic resolution' at this distance range. In the case of the alkali halide surfaces, this interaction becomes considerable at tip–surface distances less than approximately 5 Å, where the APES and the forces above cation and anion sites become different. Atomic resolution may be obtained on these surfaces in both constant force and variable-deflection modes of observation in the range of forces less than about 200 pN. When the electrostatic interaction between the tip and the surface is large, as in the case of the MgO tip and the CaO surface, good images may occur even at larger distances. However, there is a possibility that 'atomic resolution' can be obtained only in the variable-deflection mode since the tip–surface interaction has different signs above cation and anion sites (see figure 4).

In the range of the large tip–surface separations described, the surface image is unique. However, it depends on the chemical structure of the tip. The effective charge of the last atom at the end of the tip determines the qualitative character of the image. Note that in the case of cubic binary salts considered in this paper the question of the chemical identity of observed surface ions is even more complicated than for less symmetrical lattices. If different ions are non-equivalent due to crystal symmetry and surface relaxation, their identification can be much more straightforward ((1014) surface of calcite studied in [10] seems to be a good example).

When the tip–surface distance 1 Å $\leqslant d \leqslant$ 3 Å strong surface distortion is very likely, although 'atomic resolution' is still possible. However, the tip–surface interaction has a much more complicated character than that in the large-distance case. Because of the non-monotonic shape of the APES and the corresponding force curves, a given force may be encountered at two or more distinct distances of the tip from the surface (see also [8] for discussion). On this basis, one may imagine multiple 'constant force' surfaces which could in principle be imaged by a scanning AFM. Which surface the tip is imaging at any time should depend on the force, starting position (above anion or cation), thickness of the liquid layer, and the history or path of the tip reaching that point. It is possible that the tip may cross from one constant-force surface to another during scanning. Note in this regard that the relative repulsion or attraction between cation and anion sites can even change sign from one constant-force surface to another. Amongst the many instrumental or other reasons for noise in the experimental images, we should allow in principle that uncontrolled switching from one constant-force surface to another during scanning may also contribute to noise.

Another point concerns the question as to why hard covalent or semi-covalent materials have not yielded atomic periodicity in AFM as readily as have ionic, softer materials? Our present results regarding the interaction of the MgO tip with the (001) CaO surface demonstrate that it is likely that in some cases the tip cannot maintain a given nano-asperity or set of asperities long enough to generate an image. This depends on the local micro-hardness of the tip relative to the surface materials. It is interesting to note that qualitatively very similar results have been obtained recently by Tang *et al* [54] in their simulation of AFM images of the surface of graphite with a diamond tip using a standard molecular mechanics force field.

At smaller distances and when the tip penetrates the surface, atomic imaging seems much more unlikely. Dependent on the tip's chemical structure, hysteresis in the APES and the force behaviour is possible. The latter makes the meaning of 'scanning', especially in the constant-force mode, much less clear. Although we should allow in principle the possibility of periodic images, their quality will depend on the speed of relaxation process in the strongly distorted surface area around the tip. In ionic crystals, such as those considered in this paper, the ions displaced in the interstitial positions can return to the perfect lattice sites quite easily. However, the results of the present static calculations are only preliminary in this respect as they cannot account for dynamics of the surface relaxation. Note that the presence of the liquid layer or solution may cause surface dissolution and considerably affect the speed of the relaxation processes. Which crystal layer is imaged, particularly on alkali halides, still remains an open question (see also [8] for a discussion).

The results of the present study suggest that it is possible, at least in principle, to image charged impurities on the surfaces of ionic crystals. It is clear, though, that AFM information alone would be not enough to identify the impurity. However, provided there is concentration dependence and other relevant information, calculations analogous to those reported in this paper can help to identify the chemical nature of the defect.

Finally we note a qualitative agreement between the results of our calculations and the results of recent AFM study of the (1014) cleavage plane of calcite in water at room temperature [10]. Lateral atomic resolution of the oxygen sublattice was achieved in this work at very small attractive forces of the order of 10–40 pN at large tip–surface distances. In order to make our comparison more quantitative we need to use a common zero point for the tip–surface distance calculation. In [10] the $d = 0$ point was chosen as the sample position at which the transition from attractive to repulsive deflection of the lever occurred. In our results this corresponds to the distance of about 2–3 Å from the ideal surface plane. Relative to this point the calculated attractive forces of 40 pN occur at distances of 3–4 Å, which generally agree with those observed in [10].

Unfortunately more detailed comparison is presently impossible because of the difference in the crystalline structure of calcite and our materials. Note also that the experimentally observed distances and forces are determined not only by the tip–surface separation (as in our calculations), but by the thickness and elasticity of the liquid layer between the tip and the surface. Moreover, the structure of the liquid layer near the surface, which may be induced both by its interaction with the surface [55] and by dissolved ions [56] may affect the image contrast.

Acknowledgments

RTW acknowledges NSF grant DMR-9206745 for support. The authors are indebted to R W Grimes and J Binks for deriving most of the pair potentials used in this study, and

R Bell for help in the calculations. The authors are grateful to A M Stoneham, J Pethica, C R A Catlow, J L Gavartin and J D Gale for valuable discussions. The figures showing tips interacting with surfaces were generated by the MolDraw software [57]. Some of the calculations were performed on a Sun workstation at the Department of Computer Science, University of Western Australia.

References

[1] Binnig G, Quate C F and Gerber C 1986 *Phys. Rev. Lett.* **56** 930
[2] Binnig G, Gerber C, Stoll E, Albrecht T R and Quate C F 1987 *Europhys. Lett.* **3** 1281
[3] Binnig G 1992 *Ultramicroscopy* **42–44** 7
[4] Frommer J 1992 *Angew. Chem. Int. Ed. Engl.* **31** 1298
[5] Heinzelmann H, Mayer E, Brodbeck D, Overney G and Guntherodt H-J 1992 *Z. Phys. B, Condensed Mater* **88** 321
[6] Goodman F O and Garcia N 1991 *Phys. Rev.* B **43** 4728
Hartmann U 1990 *Phys. Rev.* B **42** 1541
[7] Mayer E, Heinzelman H, Brodbeck D, Overney G, Overney R, Howald L, Hug H, Jung T, Hidber H-R and Guntherodt H-J 1991 *J. Vac. Sci. Technol.* B **9** 1329
[8] Shluger A L, Wilson R M and Williams R T 1994 *Phys. Rev.* B **49** at press
[9] Marti O, Drake B, Hansma P K 1987 *Appl. Phys. Lett.* **51** 484
[10] Ohnesorge F and Binnig G 1993 *Science* **260** 1451
[11] Song K S and Williams R T 1993 *Self-Trapped Excitons* Springer Series in Solid State Sciences, vol 105 (Berlin: Springer) p 262
[12] Israelachvili J N 1985 *Intermolecular and Surface Forces* (London: Academic)
[13] Hutter J L and Bechhoefer J 1993 *J. Appl. Phys.* **73** 4123
[14] Akamine S, Barrett R C and Quate C F 1990 *Appl. Phys. Lett* **57** 316
Wolter O, Bayer Th and Greschner J 1990 *J. Vac. Sci. Technol.* **9** 1353
[15] Hoh J H, Cleveland J P, Prater C B, Revel J-P and Hansma P K 1992 *J. Amer. Chem. Soc.* **114** 4917
[16] Deitz P, Ramos C A and Hansma P K 1992 *J. Vac. Sci. Technol.* B **10** 741
[17] van Labeke D, Labani B and Girard C 1989 *Chem. Phys. Lett.* **162** 399
Girard C, van Labeke D and Vigoureux J M 1989 *Phys. Rev.* B **40** 12133
[18] Giessibl F J 1992 *Phys. Rev.* B **45** 13815
[19] Abraham F F, Batra I P and Ciraci S 1988 *Phys. Rev. Lett.* **60** 1314
Ciraci S, Baratoff A and Batra I P 1990 *Phys. Rev.* B **41** 2763
Tekman E and Ciraci S 1991 *J. Phys.: Condens. Matter* **3** 2613
Overney G, Tomanek D, Zhong W, Sun Z, Miyazaki H, Mahanti S D and Guntherodt H J 1992 *J. Phys.: Condens. Matter* **4** 4233
[20] These techniques have been reviewed in a special issue:
Catlow C R A and Stoneham A M (ed) 1985 *J. Chem. Soc., Faraday Trans. II* **85**
See also
Vitek V and Srolovitz D (ed) 1989 *Atomistic Simulation of Materials. Beyond Pair Potentials* (New York: Plenum)
[21] Luedtke W D and Landman U 1992 *Comput. Mater. Science* **1** 1
[22] Stoneham A M, Ramos M M D and Sutton A P 1993 *Phil. Mag.* A **67** 797
Ramos M M D, Sutton A P and Stoneham A M 1991 *J. Phys.: Condens. Matter* **3** S127
[23] Jenett H, Bubert H and Grallath E 1989 *Fres. Z. Anal. Chem.* **333** 502
Malgham S G 1992 *Colloids and Surfaces* **62** 87
[24] Shluger A L, Pisani C, Roetti C and Orlando R 1990 *J. Vac. Sci. Technol.* A **8** (6) 3967
Kotomin E A, Shluger A L, Causa M, Dovesi R and Ricca F 1990 *Surf. Sci.* **232** 399
[25] Gay D H and Rohl A L to be published
[26] Sauer J 1989 *Chem. Rev.* **89** 199
[27] Zhdanov S P, Kosheleva L S and Titova T I 1987 *Langmuir* **3** 960
Hoffman P and Knozinger E 1987 *Surf. Sci.* **188** 181
McFarlan A J and Morrow B A 1991 *J. Phys. Chem.* **95** 5388
Ugliengo P, Saunders V and Garrone E 1990 *J. Phys. Chem.* **94** 2260
[28] Karolewski M A and Cavell R G 1992 *Surf. Sci.* **271** 128

Goniakowski J, Bouette-Russo S and Noguera C 1993 *Surf. Sci.* **284** 315
[29] Shluger A L 1985 *Theor. Chim. Acta* (Berl.) **66** 355
Shluger A L and Stefanovich E V 1990 *Phys. Rev.* B **42** 9664
Stefanovich E V, Shidlovskaya E K, Shluger A L and Zakharov M A 1990 *Phys. Status Solidi (b)* **160** 529
[30] Shluger A L, Grimes R W, Itoh N and Catlow C R A 1991 *J. Phys.: Condens. Matter.* **3** 8027
Shluger A L, Gale J D and Catlow C R A 1992 *J. Phys. Chem.* **96** 10389
[31] Shluger A L, Kotomin E A and Kantorovich L N 1986 *J. Phys. C: Solid State Phys.* **19** 4183
Kantorovich L N 1988 *J. Phys. C: Solid State Phys.* **21** 5041
[32] Evarestov R A 1982 *Quantum-chemical Methods of Solid State Theory* (Leningrad: Leningrad University Press)
[33] Pople J A and Beveridge D L 1970 *Approximate Molecular Orbital Theory* (New York: McGraw-Hill)
[34] Tasker P W 1979 *Philos. Mag.* A **39** 119
[35] Catlow C R A and Mackrodt W C (ed) 1982 *Computer Simulation of Solids* (Berlin: Springer) vol 166
[36] Dick B G and Overhauser A W 1958 *Phys. Rev.* **112** 90
[37] Shidlovskaya E K, Stefanovich E V and Shluger A L 1988 *Soviet J. Phys. Chem.* **62** 1352
Hautman J and Klein M L 1992 *Mol. Phys.* **75** 379
[38] Mackrodt W C and Stewart R F 1979 *J. Phys. C: Solid. State Phys.* **12** 431
[39] Saul P and Catlow C R A 1985 *Philos. Mag.* **51** 107
[40] Delville A and Sokolowski S 1993 *J. Phys. Chem.* **97** 6261
[41] Grimes R W, Catlow C R A and Stoneham A M 1989 *J. Phys.: Condens. Matter* **1** 7367
[42] Fowler P W, Knowles P J and Pyper N C 1985 *Mol. Phys.* **56** 83
[43] Ziemann P J and Castelman Jr A W 1991 *J. Chem. Phys.* **94** 718
[44] Lennard-Jones J E and Dent B M 1928 *Trans. Faraday Soc.* **24** 92
[45] Kuipers L and Frenken J W M 1993 *Phys. Rev. Lett.* **70** 3907
[46] Mysovsky S, Nepomnyaschikh A and Shluger A 1987 *Optics Spectrosc.* **63** 129
Shluger A, Mysovsky S and Nepomnyaschikh A 1988 *J. Phys. Chem. Solids* **49** 1043
Shluger A, Mysovsky S and Nepomnyaschikh A 1989 *Optics Spectrosc.* **66** 599
Gavartin J, Shidlovskaya E, Shluger A and Varaksin A 1991 *J. Phys.: Condens. Matter* **3** 2237
[47] Wedding B and Klein M V 1969 *Phys. Rev.* **177** 1274
[48] Catlow C R A, Corish J, Diller K M, Jacobs P W M and Norgett M J 1976 *J. Physique* C **7** 253
[49] Gavartin J L, Catlow C R A, Shluger A L, Varaksin A N and Kolmogorov Y N 1992 *Modelling Simul. Mater. Sci. Eng.* **1** 29
[50] Stoneham A M 1989 *Physica Scripta* **T25** 17
Harding J H 1990 *Rep. Prog. Phys.* **53** 1403
[51] Vineyard G H 1957 *J. Phys. Chem. Solids* **3** 121
[52] Knox R S and Teegarden K J in 1968 *Physics of color centres* ed Fowler W B (New York: Academic)
[53] Yuan X L and McKeever S W S 1988 *Phys. Status Solidi* (a) **108** 545
[54] Tang H, Joachim C and Devillers J 1993 *Surf. Sci.* **291** 439
[55] Fölsch S, Stock A and Henzler M 1992 *Surf. Sci.* **264** 65
[56] This point has been drawn to our attention by A M Stoneham. See also
Henderson D 1988 *Ordering and organisation in ionic solutions* ed N Ise and I Sogami (London: World Scientific) p 512
[58] Cense J M 1989 *Tetrahedron Comput. Method.* **2** 65